ISSN: 2414-1895 DOI: 10.6919/ICJE.202608_12(8).0012

Numerical Analysis on Seismic Response of Buried Pipelines with Defects in Liquefiable Sites

Liang Gao, Yanhua Chen*, Mei Yang, Sainan Zhu, and Rong Wei

School of Architectural Engineering, North China University of Science and Technology, Tangshan 063210, Hebei, China

Abstract

The rapid expansion of long-distance oil and gas pipeline networks has led to increased pipeline crossings of high-seismic-risk regions. Soil liquefaction substantially degrades pipe–soil interaction restraint, triggering significant axial deformation of buried pipelines. In addition, local corrosion defects generated during long-term service reduce pipe wall cross-sectional area and induce severe stress concentration, considerably exacerbating pipeline failure hazards under seismic conditions.In this study, a finite element numerical model is established to investigate the seismic response of buried pressure pipelines with local corrosion defects in liquefiable soils. Solid elements are employed to discretize the pipeline structure, while nonlinear spring elements are adopted to characterize soil confinement effects. The stiffness degradation of soil in liquefied zones is realized by reducing the stiffness of soil springs, which accurately simulates the attenuation of soil bearing capacity during liquefaction. The maximum axial strain is selected as the critical evaluation index to quantify the tensile and compressive deformation of pipelines during liquefaction-induced uplift. By comparing the calculated axial strain with the material yield strain, the plastic development degree and bearing capacity degradation of defective pipelines can be quantitatively identified. Parametric analyses are systematically conducted to explore the effects of liquefied zone length, corrosion defect depth, and internal operating pressure on pipeline axial strain responses.The numerical results demonstrate that the expansion of the liquefied zone weakens pipe–soil constraint stiffness and enlarges pipeline axial deformation, with the maximum axial strain increasing monotonically with liquefied zone length. Deepened corrosion defects significantly reduce the local structural stiffness of the pipe wall and aggravate strain concentration at defect locations. Moreover, elevated internal pressure raises the initial circumferential stress of pipelines, which further amplifies the axial strain of defective sections under seismic excitation. This study provides a reliable theoretical reference for the seismic safety assessment and risk mitigation of defective buried pipelines in liquefaction-prone areas.

Keywords

Buried Defective Pipeline; Liquefiable Site; Seismic Excitation; Numerical Analysis.

1. Introduction

As a critical component of oil and gas storage and transportation systems, the structural integrity of buried pipelines directly determines the safety of energy transportation arteries [1]. During long-term service, coupled effects including fluctuating internal pressure, uneven foundation settlement and environmental corrosion gradually degrade pipe wall materials and form local wall thinning or geometric defects. Such defects frequently induce prominent stress concentration and drastically impair pipeline bearing capacity, which have become core hidden dangers restricting the safe service

ISSN: 2414-1895 DOI: 10.6919/ICJE.202608_12(8).0012

life of pipelines [2]. When buried pipelines traverse liquefied soil layers, the effective stress of soil disappears and peripheral pipe restraints are substantially weakened, leading to an obvious uplift tendency of pipelines under buoyancy. Subjected to seismic ground motions, pipelines will produce large dynamic bending deformation and are prone to fracture failure; the existence of local defects further concentrates structural damage and greatly increases seismic failure risks of pipelines.

Liu et al. [3] carried out analyses using the soil spring model and concluded that the seismic response of pipelines is dominated by axial strain. The maximum internal forces occur at the crown and invert of pipelines, the maximum strain appears at the interface between liquefied and non-liquefied zones, and the equivalent stress reaches its peak at pipeline mid-spans. Cao [4] constructed a 3D pipe-soil coupling model based on FLAC3D, revealed the seismic response characteristics of pipelines in three types of liquefiable sites, and proposed a liquefaction correction coefficient. He pointed out that current design codes tend to be unsafe for pipelines buried in liquefied layers and overly conservative for those in non-liquefied layers. Li et al. [5] adopted random field theory to study the influence of spatial soil variability on pipeline uplift displacement responses. They found that the average uplift displacement considering soil heterogeneity is lower than the results calculated by homogeneous soil models, and traditional random variable models cannot reasonably reflect such effects. Yang [6] utilized the Pasternak foundation model and numerical simulation to reveal the uplift response laws of straight pipes, tees and reducer pipes. The results indicated that temperature and fluid-structure coupling effects significantly amplify pipeline displacement and stress, while the influences of internal flow velocity and fluid density vary with pipe types. Xu et al. [7] proposed a stochastic dynamic analysis framework based on probability density evolution method. They demonstrated that deterministic analysis underestimates seismic risks due to randomness of earthquakes, clarified the mechanism that excess pore water pressure and seepage pressure accelerate pipeline uplift, and verified the disaster reduction effect of U-shaped gravel drainage. Chen [8] combined shaking table tests and numerical simulations to investigate the influences of liquid filling ratio, joint stiffness, site heterogeneity and internal medium type on pipeline seismic responses. He illustrated the amplification effect of pipeline responses at heterogeneous site interfaces and the mechanism of fluid-structure coupling, providing references for seismic design of buried pipelines. Wu et al. [9] conducted finite element simulations to reveal the seismic response laws of buried corroded pipelines with large elevation differences: corrosion depth exerts the most significant impact, followed by corrosion length, while corrosion width has the minimum influence. Mao et al. [10] analyzed X80 pipelines with corrosion defects via finite element methods, and found that the stress of inner-wall defects is larger than that of outer-wall defects. Stress increases with defect depth and decreases with defect radius; double defects can be regarded as independent single defects when their spacing is sufficiently large. Yu et al. [11] established a prediction method for ultimate load of X80 pipelines with corrosion defects based on finite element simulation. The maximum Mises stress appears at the transition zone of defect bottoms, and defect depth and length remarkably affect ultimate load. Verification results prove that the proposed method possesses high calculation accuracy and good applicability. Liu et al. [12] built finite element models of uniformly corroded pipelines in ANSYS Workbench, and adopted response surface methodology to screen prediction models. Defect angle imposes the strongest influence on ultimate bearing capacity, followed by depth and length, while width can be ignored. Significant interaction effects exist between length-angle and length-depth.

In summary, abundant research has focused on seismic-induced soil liquefaction, whereas few studies have investigated coupled seismic responses of pipelines in fully liquefied sites. On this basis, this paper adopts finite element numerical simulation to establish a three-dimensional finite element model of buried pipelines. The control variable method is applied to analyze the influence laws of various factors on seismic performance of defective buried pipelines, and the structural safety of buried pipelines is discussed. The research results can provide references for integrity evaluation and engineering safety assessment of buried pipelines.

ISSN: 2414-1895 DOI: 10.6919/ICJE.202608_12(8).0012

2. Establishment of Pipe-Soil Spring Model

Long-distance gas transmission pipelines are taken as the research object, and the finite element software ABAQUS is utilized to construct a three-dimensional buried pipeline model. Material parameters of the pipeline are listed in Table 1. To reproduce the actual operating state of pipelines, a uniform radial internal pressure of 6 MPa is applied to the inner pipe wall in the first analysis step according to the Code for Design of Gas Transmission Pipeline Engineering [13], as shown in Fig. 1 (arrows pointing outward from the center of the circle). Instead of establishing solid soil bodies, nonlinear spring elements are coupled to nodes on the outer pipe wall to equivalently simulate pipe-soil interaction, as displayed in Fig. 2. A rectangular groove is set at the mid-span upper part of the pipeline via local wall thinning to simulate rectangular defects induced by local corrosion, with a fixed longitudinal defect length of 90 mm, as shown in Fig. 3.

Solid elements (C3D8R, 8-node hexahedral linear reduced integration elements) are adopted for pipeline meshing to balance computational efficiency and accurate capture of local strain concentration at defects, as shown in Fig. 4. Coarse meshes are adopted in regions far away from defects, while local mesh refinement is performed near defective sections, as illustrated in Fig. 5.

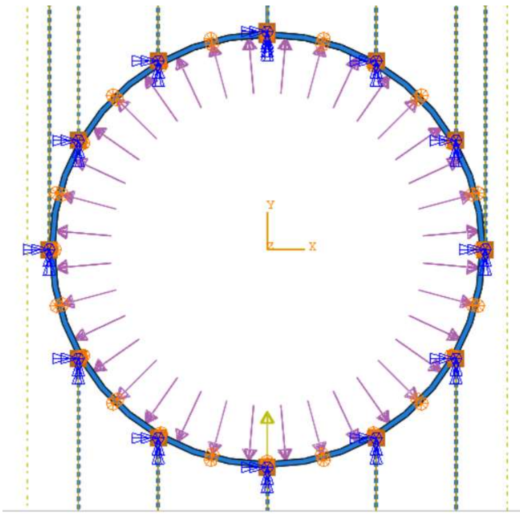

Fig. 1 Schematic diagram of internal pressure loading.

Table 1. Material Parameters of the Pipeline

Pipe	Density/(kg/m³)	Yield Strength/MPa	Young's Modulus/GPa	Poisson's Ratio	Outer Diameter/m	Wall Thickness/m
	7850	480	210	0.3	0.8	0.01

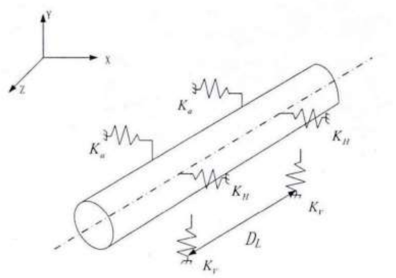

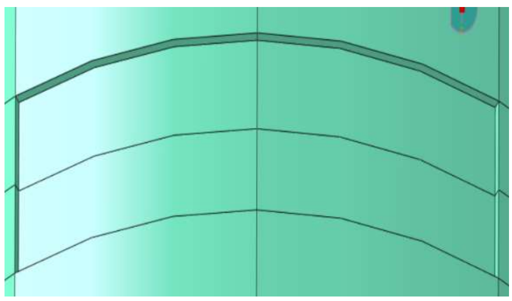

Fig. 2 Schematic diagram of the soil-spring model. **Fig. 3** Schematic diagram of corrosion defects.

ISSN: 2414-1895 DOI: 10.6919/ICJE.202608_12(8).0012

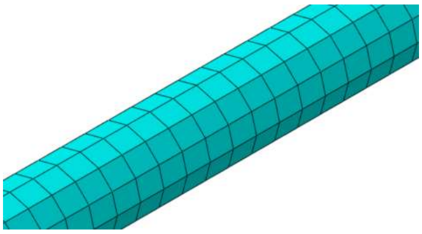
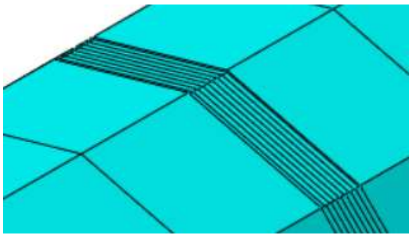

Fig. 4 Schematic diagram of pipeline meshing. **Fig. 5** Schematic diagram of meshing at the defect.

3. Stiffness of Soil Springs

The pipeline is discretized into multiple small elements, and spring elements are applied to nodes in X, Y and Z directions. Spring stiffness is calculated according to soil and pipeline properties to replace soil constraints on pipelines, forming an ideal elastoplastic pipe-soil model. Calculation formulas for soil springs are specified in the Technical Standard for Seismic Design of Oil and Gas Transmission Pipeline Routes [14].

(1)Axial Soil Sprngs of Pipelines

$$\mathrm{f_s} = pD\alpha_b c_b + \pi DH\gamma_\mathrm{b}\frac{1+K_{0\mathrm{b}}}{2}\tan\delta_\mathrm{b} \tag{1}$$

$$\alpha_\mathrm{b} = 0.608 - 0.12\mathrm{c_b} - \frac{0.274}{\mathrm{c_b^2}+1} + \frac{0.695}{\mathrm{c_h^3}+1}, \tag{2}$$

$$\delta_\mathrm{b} = \mathrm{f}\varphi_\mathrm{b} \tag{3}$$

Where:

D – outer diameter of the pipeline

α_b – adhesion factor

$\mathrm{c_b}$ – cohesion of the trench backfill soil

H – distance from the ground surface to the pipeline centerline

γ_b – effective unit weight of overburden soil

$K_{0\mathrm{b}}$ – at-rest earth pressure coefficient of the overburden soil

δ_b – interface friction angle

f – friction coefficient of the external coating

(2)Horizontal Transverse Soil Springs

$$P_\mathrm{u} = N_\mathrm{ch}\mathrm{c}D + N_\mathrm{qh}\rho_\mathrm{sl}\mathrm{g}HD \tag{4}$$

$$X_\mathrm{u} = 0.04(H + \frac{D}{2}) \tag{5}$$

ISSN: 2414-1895
DOI: 10.6919/ICJE.202608_12(8).0012

$$N_{\mathrm{ch}} = 6.752 + 0.065\frac{H}{D} - \frac{11.063}{(\frac{H}{D}+1)^2} + \frac{7.119}{(\frac{H}{D}+1)^3} \tag{6}$$

$$N_{\mathrm{qh}} = C_0 + C_1(\frac{H}{D}) + C_2(\frac{H}{D})^2 + C_3(\frac{H}{D})^3 + C_4(\frac{H}{D})^4 \tag{7}$$

Where:

P_{u} – horizontal lateral soil pressure on the pipeline

X_{u} – lateral soil spring yield displacement

N_{ch} – calculation parameters of soil cohesion

c – where c is the soil cohesion

N_{qh} – coefficient related to the internal friction angle of soil

φ – internal friction angle of soil

ρ_{sl} – density of the surrounding soil

(3)Upward Vertical Soil Springs

$$\mathrm{q_u} = N_{\mathrm{cvu}}\mathrm{c}D + N_{\mathrm{qvu}}\rho_{\mathrm{sl}}\mathrm{g}DH \tag{8}$$

$$Y_{\mathrm{u}} = (0.01 - 0.02)\ H \tag{9}$$

$$N_{\mathrm{cvu}} = 2(\frac{H}{D}) \tag{10}$$

$$N_{\mathrm{qvu}} = (\frac{\varphi}{44})(\frac{H}{D}) \tag{11}$$

Where:

$\mathrm{q_u}$ – vertical earth pressure on the pipeline

Y_{u} – vertical soil spring yield displacement

N_{cvu} – parameters accounting for soil cohesion

N_{qcv} – coefficient related to the internal friction angle of soil for the vertical direction

(4)Downward Vertical Soil Springs

$$\mathrm{q_{ul}} = N_{\mathrm{cvd}}\mathrm{cD} + N_{\mathrm{qvd}}\rho_{\mathrm{sl}}\mathrm{g}HD + N_{\gamma}\rho_{\mathrm{sl}}\mathrm{g}D^2/2 \tag{12}$$

$$Y_{\mathrm{ul}} = 0.1D \tag{13}$$

$$N_{\mathrm{cvd}} = [\cot(\varphi + 0.001)]\{e^{\pi\tan(\varphi+0.001)}[\tan(45 + \frac{\varphi + 0.001}{2})]^2 - 1\} \tag{14}$$

ISSN: 2414-1895 DOI: 10.6919/ICJE.202608_12(8).0012

$$N_{\mathrm{qvd}} = \mathrm{e}^{\pi\tan\varphi}[\tan(45+\frac{\varphi}{2})]^2 \tag{15}$$

$$N_{\gamma} = \mathrm{e}^{0.18\varphi\text{-}2.5} \tag{16}$$

Where:

q_{ul} – downward soil pressure on the pipe

Y_{ul} – downward yield displacement of the vertical soil spring

N_{cvd}、N_{qvd}、N_{λ} – parameters for the downward vertical soil spring

The whole model is divided into three regions: non-liquefied zones with 30 m length on both sides, and a liquefied zone with variable length in the middle. The physical process of sharp loss of soil bearing capacity after liquefaction is mechanically equivalent to drastic reduction of spring stiffness. Takada Shiro [15] conducted steady harmonic shaking table tests on underground pipelines to obtain buoyancy, external loads and equivalent spring constants for liquefaction analysis of buried pipelines. Combining experimental results with elastic foundation beam theory, he proposed that the equivalent spring constant of liquefied soil can be taken as 1/3000 – 1/1000 of that of non-liquefied soil for underground pipeline seismic design. In this paper, the reduction coefficient is set to 1/2000.

4. Seismic Wave Input

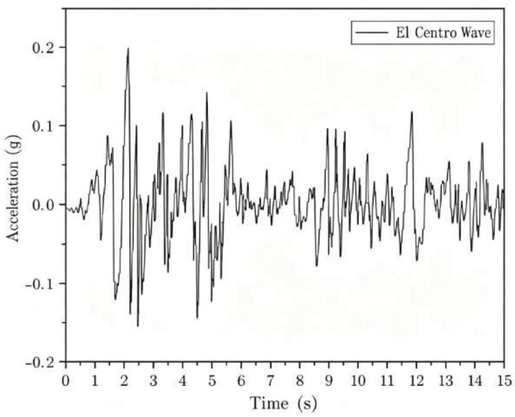

Fig. 6 Acceleration time history curve.

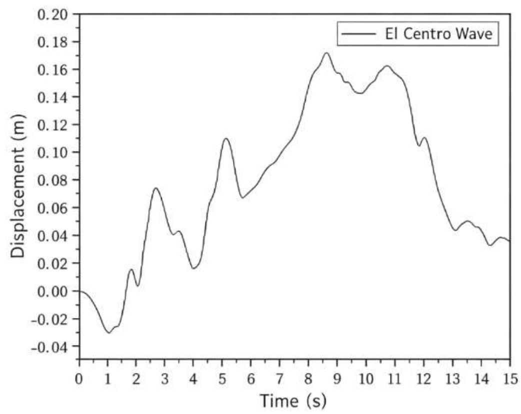

Fig. 7 Displacement time history curve.

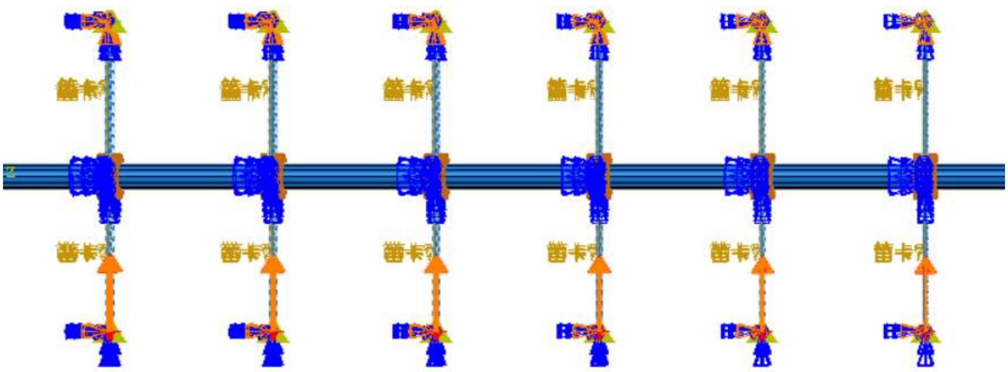

Fig. 8 Schematic diagram of ground motion application.

ISSN: 2414-1895
DOI: 10.6919/ICJE.202608_12(8).0012

After applying internal pipeline pressure, a second implicit dynamic analysis step is introduced. The El Centro seismic wave is selected, with peak ground acceleration linearly scaled to 0.2 g to avoid distortion of wave characteristics. Uniform excitation is adopted for seismic load application: the selected acceleration time-history curve (Fig. 6) is converted into a displacement time-history curve (Fig. 7), which is uniformly applied to the fixed ground ends of all soil springs, as shown in Fig. 8. Seismic ground motions act vertically upward on the pipeline along the vertical direction (the vertical upward arrow at the bottom in Fig. 8).

5. Result Analysis

The bearing capacity and deformation capacity of pipeline steel are correlated via stress-strain curves. In the elastic stage, stress is linearly proportional to strain with Young's Modulus E as the proportional coefficient. When stress exceeds yield strength, the pipeline enters the plastic stage, where strain continuously increases while stress rises slowly. Pipeline fracture failure occurs and bearing capacity is completely lost once strain reaches the ultimate strain of the material. Therefore, comparing the calculated axial strain with material yield strain can judge whether the pipeline enters the plastic state and quantify the degradation degree of bearing capacity. X70 steel is adopted in this paper, with Young's Modulus E=210 GPa, and the corresponding yield strain is calculated by Eq.

$$\varepsilon_{\mathrm{y}} = \frac{\sigma_{\mathrm{y}}}{E} = \frac{480}{210000} \approx 0.00229 \tag{17}$$

The value of 0.00229 is adopted as the critical criterion to identify plastic deformation of pipelines in subsequent analyses.

To verify the reliability of the proposed finite element model, calculation results are compared with those reported in Reference [16]. The variation laws of maximum axial strain under coupling effects of liquefied zone length and internal pressure are taken as comparison objects. Fig. 9 presents results from existing literature, and Fig. 10 shows calculation results of this paper. Both groups of curves demonstrate that the maximum axial strain nonlinearly increases with liquefied zone length, and strain responses become more significant under higher internal pressure. The consistent variation trends validate the reliability of the proposed model.

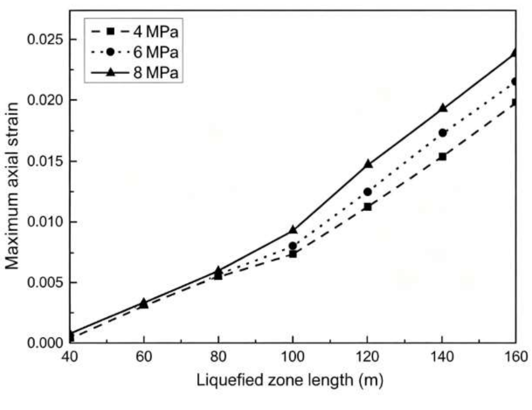

Fig. 9 Calculation Results from Existing Literature

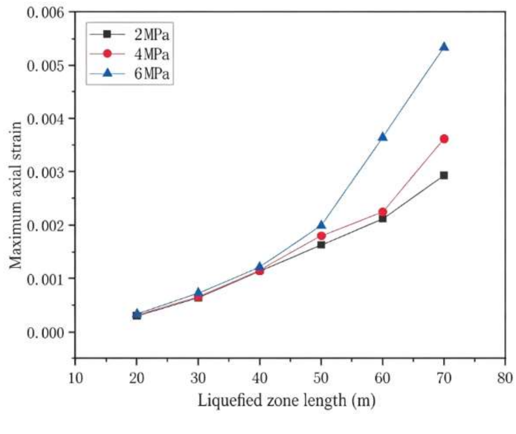

Fig. 10 Calculation Results of This Paper

5.1 Influence of Liquefied Zone Length

The control variable method is adopted, with fixed pipeline outer diameter of 0.8 m, defect depth of 4 mm and wall thickness of 10 mm. The maximum axial strain of pipelines throughout the whole

ISSN: 2414-1895 DOI: 10.6919/ICJE.202608_12(8).0012

seismic duration is extracted under liquefied zone lengths of 20 m, 30 m, 40 m, 50 m, 60 m and 70 m, as shown in Fig. 11.

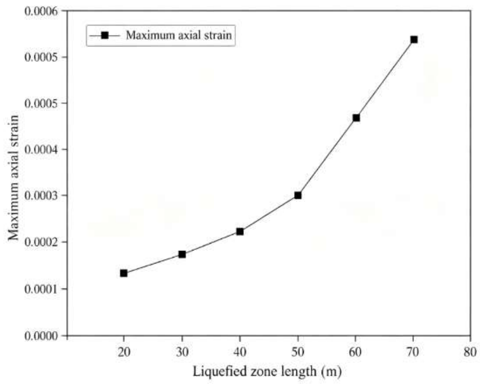

Fig. 11 Maximum Axial Strain of Pipelines under Different Liquefied Zone Lengths

It can be clearly observed from Fig. 11 that the maximum axial strain at defective sections exhibits an obvious nonlinear rising trend as the liquefied zone length expands from 20 m to 70 m. When the liquefied zone length is relatively small, anchoring restraints provided by non-liquefied soil at both ends can effectively constrain the whole liquefied segment and limit vertical bending deformation of pipelines. Therefore, when the liquefied zone length increases from 20 m to 40 m, the maximum axial strain slowly rises from approximately 0.00034 to 0.00122 with a gentle growth rate. As the liquefied zone length further increases, the coverage ratio of anchoring restraints at both ends decreases, and pipelines generate remarkable vertical deflection under coupled buoyancy and seismic loads. Accordingly, strain surges sharply when the liquefied zone length exceeds 50 m, reaching 0.00365 at 60 m and 0.00534 at 70 m, which exceeds the yield strain, indicating that the pipeline enters the plastic state with obvious bearing capacity degradation.

5.2 Influence of Defect Depth

With fixed pipeline outer diameter of 0.8 m and wall thickness of 10 mm, the maximum axial strain of pipelines with defect depths of 2 mm, 4 mm and 6 mm is analyzed under liquefied zone lengths ranging from 20 m to 70 m, as shown in Fig. 12.

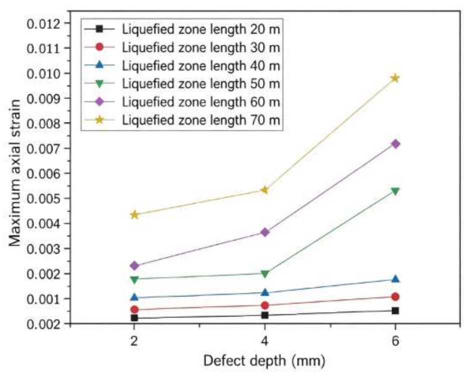

Fig. 12 Maximum Axial Strain of Pipelines under Different Defect Depths

Local wall-thinning defects break the continuity of pipeline cross-sections, and defective zones become high-risk areas of strain concentration under seismic loads. As illustrated in Fig. 12, strain values remain relatively low under a defect depth of 2 mm, and the strain approaches yield strain only when the liquefied zone length exceeds 60 m. When the defect depth increases to 4 mm, strain levels

ISSN: 2414-1895 DOI: 10.6919/ICJE.202608_12(8).0012

rise significantly and exceed yield strain for liquefied zones longer than 50 m. When the defect depth reaches 6 mm, strain surges drastically: the strain reaches 0.0053 at a liquefied zone length of 50 m and rises to 0.00988 at 70 m, which means the pipeline undergoes severe plastic deformation and substantial bearing capacity loss. In addition, the location of peak strain migrates with varying defect depth and liquefied zone length. As listed in Table 2, when the defect depth is 2 mm, peak strain occurs at defective sections for a liquefied zone length of 20 m, and shifts to the interface between liquefied and non-liquefied zones once the liquefied zone length exceeds 30 m. This indicates that global bending deformation induced by liquefied zone length dominates structural responses under shallow defects. When the defect depth increases to 4–6 mm, peak strain mostly appears at defective sections, which become the critical parts controlling pipeline safety.

Table 2. Maximum Axial Strain and Corresponding Locations under Different Defect Depths

Defect Depth(mm)	Liquefied Zone Length(m)	Maximum Axial Strain at Defect	Maximum Axial Strain at Interface	Location of Maximum Axial Strain
2	20	0.00024	0.00022	Defect
4	20	0.00034	0.00022	Defect
6	20	0.00053	0.00022	Defect
2	30	0.00055	0.00057	Interface
4	30	0.000731	0.00057	Defect
6	30	0.00107	0.00057	Defect
2	40	0.00093	0.00104	Interface
4	40	0.00121	0.00104	Defect
6	40	0.00174	0.00104	Defect
2	50	0.00155	0.0018	Interface
4	50	0.00199	0.0018	Defect
6	50	0.0053	0.0018	Defect
2	60	0.00187	0.00231	Interface
4	60	0.00365	0.00231	Defect
6	60	0.00717	0.00231	Defect
2	70	0.00212	0.00437	Interface
4	70	0.00534	0.00437	Defect
6	70	0.00988	0.00437	Defect

5.3 Influence of Internal Pipeline Pressure

The pipeline outer diameter is fixed at 0.8 m, wall thickness at 10 mm and defect depth at 4 mm. The maximum axial strain of pipelines under internal pressures of 2 MPa, 4 MPa and 6 MPa is analyzed for liquefied zone lengths ranging from 20 m to 70 m, as shown in Fig. 13.

The amplification effect of internal pressure on maximum axial strain is significantly regulated by liquefied zone length. When the liquefied zone length is less than 60 m, the strain increases slightly as internal pressure rises from 2 MPa to 6 MPa, and internal pressure exerts a weak influence; all strain values under such working conditions are lower than yield strain. When the liquefied zone length reaches or exceeds 60 m, increasing internal pressure leads to a sharp rise in axial strain. For a liquefied zone length of 60 m, the strain jumps from 0.00207 to 0.00365; for 70 m, the strain rises

 Volume 12 Issue 8, 2026
DOI: 10.6919/ICJE.202608_12(8).0012

from 0.00234 to 0.00534, far exceeding yield strain, presenting a strong nonlinear coupling relationship between the two parameters.

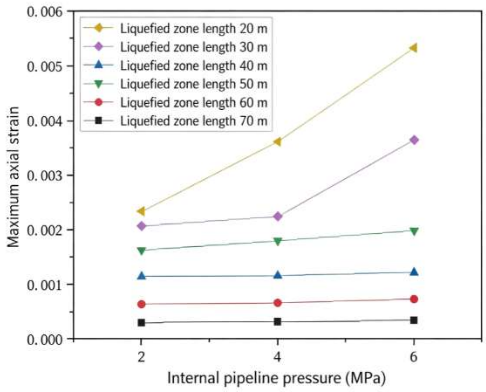

Fig. 13 Maximum Axial Strain of Pipelines under Different Internal Pressures

The location of peak strain also migrates with varying internal pressure. As shown in Table 3, under an internal pressure of 2 MPa, peak strain occurs at defective sections for liquefied zones shorter than 50 m, and shifts to the interface for lengths over 60 m. When internal pressure rises to 4 MPa and 6 MPa, peak strain always appears at defective sections, which demonstrates that high internal pressure aggravates local strain concentration at defects, making defective zones dominate the peak structural response of pipelines.

Table 3. Maximum Axial Strain and Corresponding Locations under Different Internal Pressures

Internal Pressure(MPa)	Liquefied Zone Length(m)	Maximum Axial Strain at Defect	Maximum Axial Strain at Interface	Location of Maximum Axial Strain
2	20	0.00030	0.00021	Defect
4	20	0.00032	0.00021	Defect
6	20	0.00034	-0.00022	Defect
2	30	0.00063	-0.00053	Interface
4	30	0.000662	-0.00053	Defect
6	30	0.000731	-0.00057	Defect
2	40	0.001147	0.001038	Interface
4	40	0.001165	0.001003	Defect
6	40	0.001218	0.001049	Defect
2	50	0.00163	0.00156	Interface
4	50	0.0018	0.00167	Defect
6	50	0.00199	0.00179	Defect
2	60	0.00207	0.00212	Interface
4	60	0.00225	0.00222	Defect
6	60	0.00365	0.00231	Defect
2	70	0.00234	0.00293	Interface
4	70	0.00362	0.00331	Defect
6	70	0.00534	0.00436	Defect

ISSN: 2414-1895 DOI: 10.6919/ICJE.202608_12(8).0012

6. Conclusion

A pipe-soil spring analysis model is established to investigate the influencing factors of maximum axial strain of defective buried pipelines in liquefiable sites, and the main conclusions are summarized as follows:

(1)Liquefied zone length imposes a significant nonlinear amplification effect on pipeline axial strain. Strain grows slowly when the liquefied zone length is less than 40 m, and surges sharply once the length exceeds 50 m. Taking the yield strain of X70 steel as the criterion, pipelines enter the plastic state with degraded bearing capacity when the liquefied zone length exceeds 60 m. Deformation verification based on strain criteria is recommended for buried pipelines crossing long liquefied zones.

(2) The location of peak strain migrates with different parameter combinations. Under shallow defects or low internal pressure, peak strain shifts from defective sections to the interface between liquefied and non-liquefied zones for long liquefied zones. For deep defects or high internal pressure, peak strain always occurs at defective sections. Both defective zones and liquefaction interfaces should be focused on in seismic design, and the most dangerous position should be determined according to actual pipeline operating conditions.

(3) Defect depth remarkably amplifies local stress and strain responses of pipelines. The peak strain at defective sections continuously rises as the defect depth increases from 2 mm to 6 mm, with a nonlinear growth rate accelerating with depth. Corrosion defects with depth exceeding 20% of wall thickness should be prioritized during pipeline inspection, and their influences on seismic safety should be evaluated timely.

(4) The influence of internal pipeline pressure on maximum axial strain strongly depends on liquefied zone length. When the liquefied zone length is less than 60 m, the maximum axial strain only slightly increases as internal pressure rises from 2 MPa to 6 MPa; strain surges drastically once the length exceeds 60 m. Internal pressure effects must be incorporated in seismic verification for high-pressure pipelines crossing long liquefied zones, while internal pressure can be neglected as a primary sensitive parameter for pipe segments with short liquefied zones.

Acknowledgments

Natural Science Foundation of Hebei Province (No. E2020209072);

Applied Basic Research Project of Tangshan Science and Technology Bureau (No. 22130211H).

References

[1] Wang, Y. X., Yi, X. Z., He, Y. X., et al. (2025). Residual strength prediction of X80 oil and gas pipelines with complex corrosion defects. *Petroleum Machinery*, 53(8), 116–124. (In Chinese)

[2] Pu, F., Yang, Y. B., & Fan, X. (2026). Failure pressure evaluation of pipelines under interaction of multiple corrosion defects. *Oil & Gas Storage and Transportation*, 1–19. (In Chinese)

[3] Liu, C. G., & Ke, G. M. (2010). Numerical simulation analysis of buried pipelines in liquefied zones. *Earthquake Engineering and Engineering Vibration*, 30(4), 156–162. (In Chinese)

[4] Cao, X. D. (2025). Seismic response analysis of buried continuous steel pipelines in liquefiable sites with different soil layer structures [Master's thesis]. Institute of Engineering Mechanics, China Earthquake Administration. (In Chinese)

[5] Li, D. Q., Shan, S. Z., Wang, S., & Du, W. Q. (2024). Uplift response and vulnerability analysis of buried pipelines in liquefied zones considering spatial variability of soil. *Engineering Mechanics*, 41(9), 31–41. (In Chinese)

[6] Yang, C. S. (2022). Theoretical analysis and finite element simulation of pipeline structures in liquefied soil layers [Master's thesis]. Jinan University. (In Chinese)

[7] Xu, B., Chen, K. H., Wang, L. L., et al. (2024). Stochastic seismic response analysis and reliability evaluation of pipelines in liquefied soil. *Chinese Journal of Geotechnical Engineering*, 46(1), 81–89. (In Chinese)

ISSN: 2414-1895 DOI: 10.6919/ICJE.202608_12(8).0012

[8] Chen, H. Y. (2024). Shaking table tests and influencing factor research on seismic response of buried pipelines [Master's thesis]. Guangzhou University. (In Chinese)

[9] Wu, Y., Li, D., & Chen, L. (2023). Seismic response research of buried X80 pipelines with corrosion defects at large elevation differences. *Petroleum Machinery*, 51(4), 144–154. (In Chinese)

[10] Mao, R., Zhan, S. D., & Zhang, J. (2025). Stress analysis of X80 pipelines with inner and outer wall corrosion defects. *Journal of Beibu Gulf University*, 40(2), 57–64. (In Chinese)

[11] Yu, L., & Kong, L. Z. (2025). Simulation and prediction of ultimate load of X80 oil and gas pipelines with corrosion defects. *Mechanics in Engineering*, 47(2), 323–330. (In Chinese)

[12] Liu, Q., Zhang, M., & Zhang, Q. (2023). Influence analysis of corrosion defect parameters on ultimate bearing capacity of pipelines. *Chemical Safety and Environment*, 36(9), 40–44. (In Chinese)

[13] Ministry of Housing and Urban-Rural Development of the People's Republic of China. (2015). *Code for Design of Gas Transmission Pipeline Engineering (GB 50251-2015)*. China Planning Press. (In Chinese)

[14] Ministry of Housing and Urban-Rural Development of the People's Republic of China. (2017). *Technical Standard for Seismic Design of Oil and Gas Transmission Pipeline Routes (GB/T 50470-2017)*. China Planning Press. (In Chinese)

[15] Takada, S. (1988). *Earthquake Resistance of Buried Pipelines*. Academic Books and Periodicals Press. (In Chinese and English)

[16] Bing, Q. Y. (2018). Mechanical response research of buried liquid transport pipelines under site liquefaction [Master's thesis]. North China University of Science and Technology. (In Chinese)